# Feasibility Studies of EMTP Simulation for the Design of the Pulsed-Power Generator Using MPC and BPFN for Water Treatments

Jaegu Choi, *Member, IEEE*, Takahiro Yamaguchi, Kunihiro Yamamoto, Takao Namihira, *Senior Member, IEEE*, Takashi Sakugawa, *Member, IEEE*, Sunao Katsuki, *Member, IEEE*, and Hidenori Akiyama, *Fellow, IEEE*

***Abstract*—In this paper, a pulsed-power generator that consists of a magnetic pulse compressor (MPC) and a Blumlein-type pulse forming network (BPFN) has been developed. The pulsed-power generator can be operated with high repetition rate, long lifetime, and high reliability for water treatments such as sterilization of microorganisms, decomposition of harmful materials, and ozone generation. An informative explanation about the simulation methodology using electromagnetic transient program was presented in order to give guidance for more efficient design of the pulsed-power generator with MPC and BPFN. The comparison study of the simulation result with the experimental result was carried out. As a result, it was found that the simulation results and the experimental results with the manufactured MPC and BPFN showed a reasonable agreement. In addition, a large volume of streamer discharge was successfully generated in water with the developed system.**

***Index Terms*—Blumlein-type pulse forming network (BPFN), electromagnetic transient program (EMTP), magnetic pulse compressor (MPC), pulsed power, water treatments.**

## I. Introduction

SINCE MELVILLE described a magnetic pulse compressor (MPC) by using the nonlinear permeability of ferromagnetic materials in 1951 [1] as a cornerstone for the high repetition rate pulsed-power generators, research on MPC has focused on high-power pulse generation such as radar modulation, nuclear particle acceleration, and impulse testing for a long time [2].

Recent developments of ferromagnetic materials [3], [4] and semiconductor switches with excellent characteristics have allowed the high repetitive operation of magnetic switches (MS) with very low loss and have made it possible to use the repetitive pulsed power generated by MPC on practical industrial applications such as laser exciters, decomposition of harmful gases, removal of volatile toxic compounds, and water treatments [5]–[8] due to its high repetition rate, high stability, and long lifetime.

Meanwhile, there are numerous applications in both physics and electrical engineering for short ($t_{\rm p} < 10\ \mu$s) electrical pulses. These applications often require that the pulses have a good square shape, i.e., they have fast rise and fall times ($t_{\rm r}$, $t_{\rm f} \ll t_{\rm p}$) [9]. Although there are many ways for generating such pulses, pulse forming network (PFN) is one of the simplest techniques. The Blumlein-type PFN (BPFN) is very popular due to the fact that the power supply used to charge the network has the same output potential as the required pulse amplitude.

Although there has been much need for the design and analysis techniques of the high repetition rate pulsed-power generator using MPC and BPFN, there has been few studies concerning the simulation methodology of the MPC [10] and the BPFN, probably due to the difficulties in the design of the nonlinear permeability of ferromagnetic cores for MS and pulse transformer (PT).

In this paper, a pulsed-power generator that can be operated with high repetition rate, long lifetime, and high reliability for industrial applications has been developed. An informative explanation about the simulation methodology using electromagnetic transient program (EMTP) [11], [12] was given in order to give guidance for more efficient design of the pulsed-power generator with MPC and BPFN. The comparison study of the simulation result with the experimental result was carried out. Therefore, the proposed methodology is expected to contribute to the design of the nonlinear devices in the pulsed-power field as well.

## II. Fundamental Theory

Fig. 1 illustrates a typical MPC circuit [9]. Suppose that $C_1 = C_2 = C_3 = C$ and $\mathrm{MS_s} \ll L_1 \ll \mathrm{MS_u}$. $\mathrm{MS_u}$ and $\mathrm{MS_s}$ refer to the unsaturated inductance and the saturated inductance of the MS, respectively. On switch closure with the above conditions, the charged energy in $C_1$, which is initially charged to a potential $V_0$, is transferred to $C_2$ by $C{-}L{-}C$ resonance. As the potential on $C_2$ reaches a point at which MS will saturate, the energy transfer takes place from $C_2$ to $C_3$ once more. In the latter loop, $L_1$ and the switch are replaced by the MS. The voltage $V_1$ and the current $I_1$ are compressed to $V_2$ and $I_2$, respectively, by the function of MS during the energy transfer, as shown in Fig. 1(b).

Considering the charging of capacitor $C_2$ from the previous capacitor $C_1$ via the inductor $L_1$, the voltage $V_1(t)$ on $C_2$ will be given by

$$V_1(t) = V_0 \frac{C_1}{C_1 + C_2}(1 - \cos \omega t) = \frac{V_0}{2}(1 - \cos \omega t) \qquad (1)$$

Manuscript received September 23, 2005; revised December 6, 2005. This work was supported by Kumamoto University 21st Century Center of Excellence (COE) Program, Pulsed Power Science and its Application.

The authors are with the Department of Electrical and Computer Engineering, Kumamoto University, Kumamoto 860-8555, Japan (e-mail: jgchoi@st.eecs.kumamoto-u.ac.jp).

Color versions of Figs. 3–14 are available online at http://ieeexplore.ieee.org.
Digital Object Identifier 10.1109/TPS.2006.883384

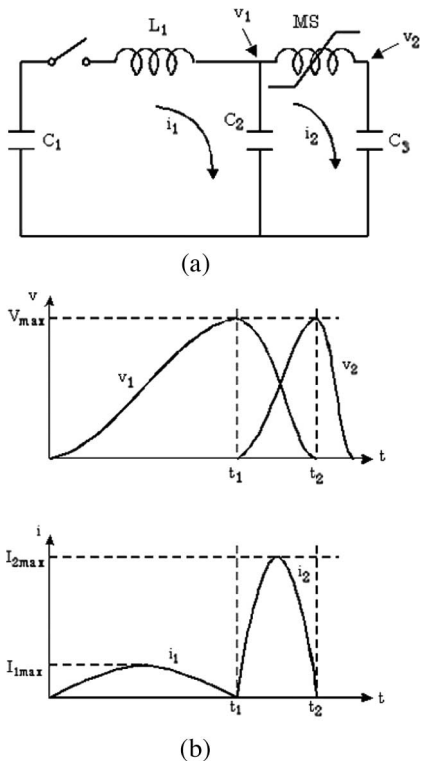


Fig. 1. Operation of the basic MPC. (a) Basic MPC circuit. (b) Voltage and current waveforms.

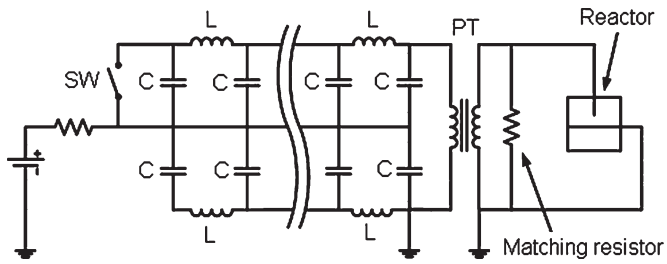


Fig. 2. Diagram of the BPFN.

where $\omega = 1/\sqrt{L_1 C_0}$. The time $t$ to charge $C_2$ is given by

$$t = \pi\sqrt{L_1 C_0} \tag{2}$$

where $C_0 = C_1 C_2/(C_1 + C_2) = C/2$.

As a result, the maximum voltage on $C_3$ is equal to the charging voltage $V_0$ on $C_1$, and the voltage amplification does not occur. The current amplification ratio $\eta_c$ is given by

$$\eta_c = \frac{I_{2\max}}{I_{1\max}} = \frac{V_0\sqrt{\frac{C_0}{\mathrm{MS}_s}}}{V_0\sqrt{\frac{C_0}{L_1}}} = \sqrt{\frac{L_1}{\mathrm{MS}_s}}. \tag{3}$$

Fig. 2 describes a typical BPFN that consists of *L–C* ladder networks. In this circuit, with closing of SW, the charged energy in each capacitor begins to propagate in the BPFN circuit to form a given pulsewidth at the load. The PT was attached to the network in order to obtain a higher output voltage. It is possible to control the pulsewidth of the output pulse voltage by varying the number of the units of the inductor and the capacitor in the BPFN. The pulsewidth $\tau$ is given by

$$\tau = 2N\sqrt{LC} \tag{4}$$

where $N$ refers to the number of units. The characteristic impedance of the *L–C* ladder network is given by

$$Z = \sqrt{\frac{L}{C}}. \tag{5}$$

On the other hand, the load impedance for BPFN is given by $2Z$.

## III. Pulsed-Power System Components

The block diagram of the developed repetitive pulsed-power system is presented in Fig. 3. The system consists of the MPC unit, the BPFN unit, and the load unit. In this paper, the voltages and the currents at each point were measured in order to compare the experimental results with the simulated results. In this paper, the system was operated with the repetition rate of 30 pps and average power of 1.2 kW. The applied voltage and the discharge current through the needle to plane electrodes were measured using the voltage divider (EP-100K, Pulse Electronic Engineering Company, Japan) and the current monitor (Model 110A, Pearson Electronics, Japan), respectively. The oscilloscope (HP54542A, Hewlett-Packard, USA) recorded the single-shot signals from the measurement devices.

### A. MPC Unit

The MPC unit consists of a charger, low-inductance capacitors ($C_0$, $C_1$), saturable inductors ($\mathrm{SI}_0$, $\mathrm{SI}_1$), a gate-turn-off thyristor (GTO) and a PT (PT1). The charger is a high-voltage power supply using resonant inverter (202 A, LAMBDA EMI). The average charging rate of the charger is 2000 J/s (Joules per second). The capacitances of $C_0$ and $C_1$ are 6.6 $\mu$s and 200 nF, respectively. Fe-based nanocrystalline magnetic cores (FT-1H, Hitachi metals Ltd.) were used as the MSs ($\mathrm{SI}_0$, $\mathrm{SI}_1$). GTO is a high-speed thyristor for pulsed-power application (5STH20H4501, ABB). The shortcoming of spark gap switches, that is, deterioration of the gap can be overcome by using this solid state switch. The magnetic assist by the saturable inductor ($\mathrm{SI}_0$) follows the GTO switching. The magnetic assist has the effect of reducing the switching loss of GTO [4]. In this paper, it was possible to reduce the switching loss by about 23% by the magnetic assist. MPC that consists of the MS and the solid state switch can be operated with higher repetition rate, longer lifetime, and higher reliability than conventional ones. PT1 has a function of step-up transformer with the voltage gain of six (winding ratios 4 : 24). The losses of GTO, $\mathrm{SI}_0$, PT1, $\mathrm{SI}_1$, and $\mathrm{SI}_2$ were obtained as 60, 10, 9, 12, and 22 W, respectively, by the calculation method in the earlier paper [3].

Fig. 4 shows the measured waveforms of $V_0$, $V_1$, $I_0$, and $I_1$, respectively. GTO turns on after $C_0$ is fully charged up to 3.6 kV by the charger, and then $\mathrm{SI}_0$ saturates immediately after the assist time. The current $I_0$ with duration of 4.4 $\mu$s flows in the primary circuit of PT1. As a result, $C_1$ is charged to a high

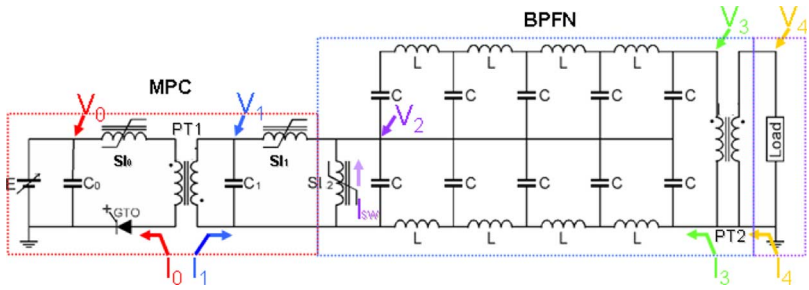


Fig. 3. Schematic diagram of the pulsed-power generator for water treatments.

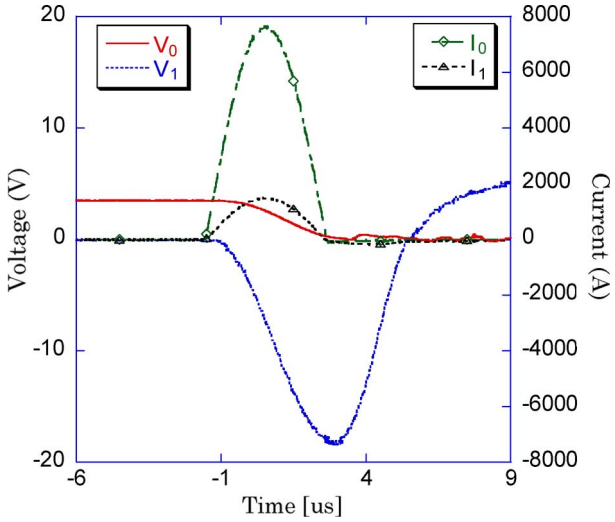


Fig. 4. Measured waveforms of $V_0$, $V_1$, $I_0$, and $I_1$.

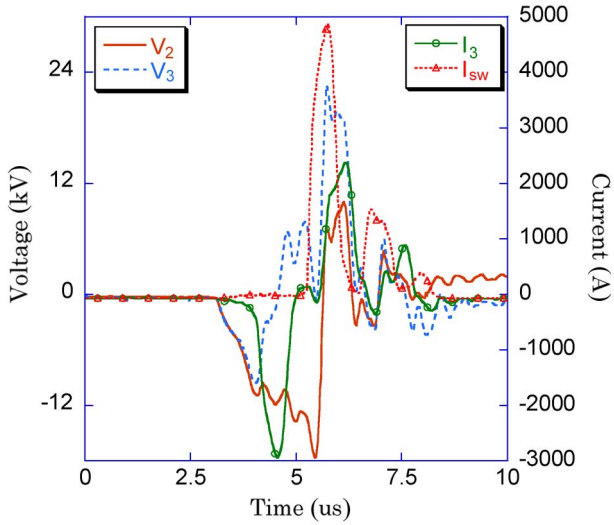


Fig. 5. Measured waveforms of $V_2$, $V_3$, $I_3$, and $I_{\rm sw}$.

voltage through the PT1. At this time, $SI_1$ performs as a current blocking inductor during the charging time for $C_1$, whereas it acts as a low-inductance switch during the discharging time. It should be noted in the figure that $V_1$ reached no more than 18 kV due to the aforementioned losses in the circuit.

### B. BPFN Unit

The BPFN unit consists of ceramic capacitors, inductors, an MS $(SI_2)$, and a high-voltage step-up PT (PT2). The voltage gain of PT2 is six (winding ratio, primary: secondary $= 1:6$). MPC is used as a charging generator for BPFN. BPFN is charged by MPC output current. The maximum BPFN charging voltage is about $-20$ kV. The capacitance and the inductance of each stage in the BPFN are 20 nF and 500 nH, respectively. Therefore, BPFN was designed to have the characteristic impedance of 5 $\Omega$ and the output pulsewidth of 1 $\mu$s. Fig. 5 shows the measured voltage and current waveforms of $V_2$, $V_3$, $I_3$, and $I_{\rm sw}$, respectively. In this figure, the waveforms are synchronized to those in Fig. 4. The charging process and the resultant output voltage of BPFN can be observed as $V_2$ and $V_3$, respectively, although the waveforms look complicated due to the stray components in BPFN.

### C. Load Unit

The load unit consists of the point to plane electrode and the noninductive resistor of 360 $\Omega$ in parallel. The latter is matched to the characteristic impedance of the BPFN unit. The needle to plane geometry electrode that immersed into tap water (conductivity: 25 mS/m) was used as the discharge electrode in this paper. The radius of curvature at the needle tip was 30 $\mu$m. The distance between the tip of the needle electrode and the plane electrode was fixed at 100 mm.

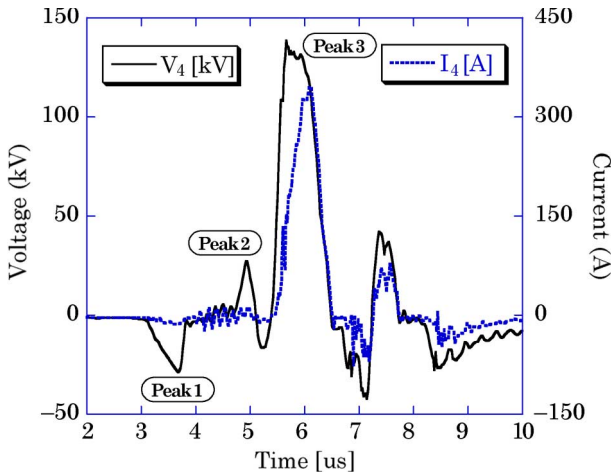


Fig. 6. Measured waveforms of $V_4$ and $I_4$.

Fig. 6 shows the typical waveforms of the output voltage and current from PT2. The output voltage $V_4$ has three inherent peaks, that is, Peak 1, Peak 2, and Peak 3. Peak 1 is due to

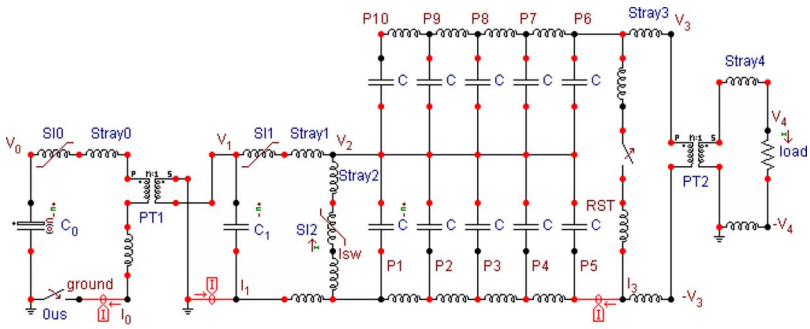


Fig. 7. Schematic diagram of the EMTP simulation circuit for the pulsed-power generator.

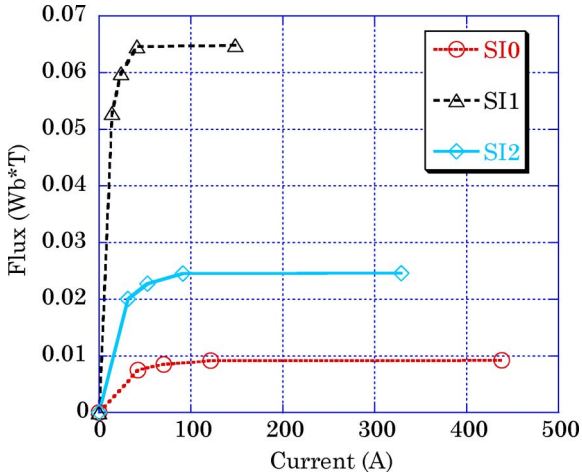


Fig. 8. Flux and current relationships for MSs at a saturation time of 0.5 $\mu$s.

the fact that the reset circuit is adopted for the maximal flux swing of PT2, and that the peak appears until the core saturates in the negative direction. Peak 1 is undesirable but unavoidable. Peak 2 originates from the nonuniform charging over the BPFN capacitors. This will be dealt with in the following section. Peak 3 is the main output voltage peak. It is observed that the peak voltage, rise time, and pulsewidth (FWHM) are about 140 kV, 200 ns, and 1 $\mu$s, respectively.

## IV. EMTP Simulation Results

In this paper, EMTP was used to analyze the transient phenomena of the high-repetition rate pulsed-power generator with nonlinear elements such as the magnetic cores. Fig. 7 shows the schematic diagram of the EMTP simulation circuit for the pulsed-power generator, which is originally based on that of Fig. 3.

Fig. 8 shows the flux and current relationships for magnetic cores, SI0, SI1, and SI2, respectively. The curves were derived from the B–H curves of the same magnetic core using the following relationship

$$\Phi = n \cdot B \cdot A \text{ and } I = H \cdot l/n \tag{6}$$

where $\Phi$ is the flux [Wb · T], $n$ is the number of turns [T], $B$ is the flux density [Wb/m$^2$], $A$ is the sectional area of the core [m$^2$], $I$ is the current [A], $H$ is the magnetic field [A · T/m], and $l$ is the average length of the magnetic path of the core [m].

TABLE I
Calculated Inductances of the MSs for EMTP Simulation

| | SI0 | SI1 | SI2 |
|---|---|---|---|
| Lu | 0.18 mH | 3.7 mH | 0.63 mH |
| Ls | 0.08 μH | 1.64 μH | 0.28 μH |

TABLE II
Stray Inductances Used in the EMTP Simulation Circuit

| Stray $L_0$ | Stray $L_1$ | Stray $L_2$ | Stray $L_3$ | Stray $L_4$ |
|---|---|---|---|---|
| 0.50 μH | 0.35 μH | 0.16 μH | 1.50 μH | 90 μH |

From the derived flux–current curves, it is possible to calculate the unsaturated inductances and the saturated inductances of the MSs. The results are presented in Table I. The ratio of the unsaturated inductance to the saturated inductance is 2240, which is due to the fact that the unsaturated relative permeability $\mu_{\rm ru}$ and the saturated relative permeability $\mu_{\rm rs}$ are calculated to 4480 and 2, respectively. It should be noted that this big difference plays an important role as a switch in the MPC circuit.

Before the performance verification of EMTP in comparison with the experimental results, the authors checked the stray inductances in the circuit, as shown in Table II. Stray inductances $L_0$, $L_1$, $L_2$, $L_3$, and $L_4$ were minimized as low as possible when the pulsed-power generator was manufactured. However, stray inductance $L_4$ showed quite a high value of 90 $\mu$H due to the long line to the load.

Fig. 9 shows the simulated waveforms of $V_0$, $V_1$, $I_0$, and $I_1$, respectively. In the figure, the energy transfer from $C_0$ to $C_1$ can be observed in the same way as Fig. 4. The simulation results show a reasonable agreement with the experimental ones considering that there exist numerous nonlinear elements and stray components in the system. However, it should be noted that the pulsewidth of $I_0$ is longer than that in Fig. 4 by 25%. This means that the value of the saturated relative permeability in the actual magnetic core is less than two, whereas the pulsewidth of the current is given by the form of (2), and the value of the saturated relative permeability in the modeled magnetic core is two.

Fig. 10 shows the simulated waveforms of $V_2$, $V_3$, $I_3$, and $I_{\rm sw}$, respectively. In the figure, the output voltage of the BPFN $V_3$ can be determined from the difference between the voltage

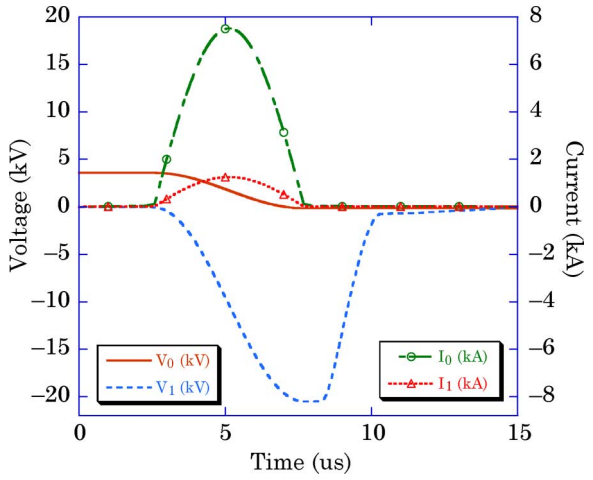


Fig. 9. Simulated waveforms of $V_0$, $V_1$, $I_0$, and $I_1$.

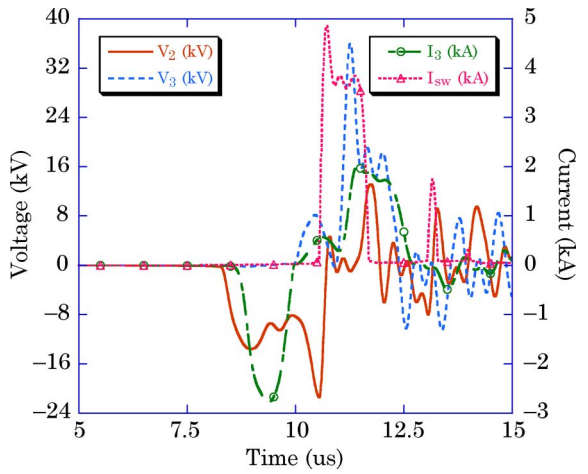


Fig. 10. Simulated waveforms of $V_2$, $V_3$, $I_3$, and $I_{\rm sw}$.

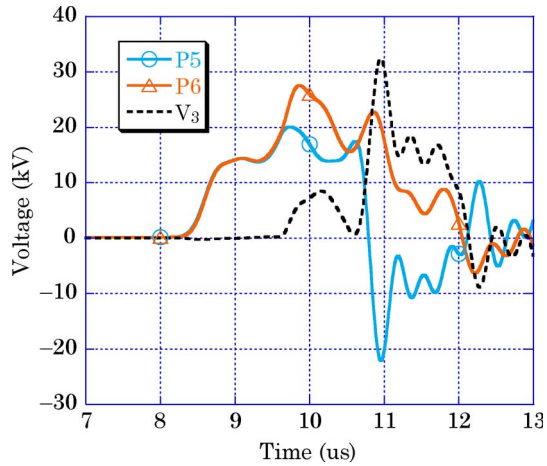


Fig. 11. Simulated voltage waveforms at point P5, P6, and $V_3$.

at P6 and the voltage at P5 (in this case, stray inductance 3 can be neglected). Fig. 11 explains the generation of Peak 2 and the output voltage $V_3$. The output pulse has the pulsewidth of 1 $\mu$s, and the combination of the inductors and capacitors in BPFN is generating higher peak voltage than the charging voltage.

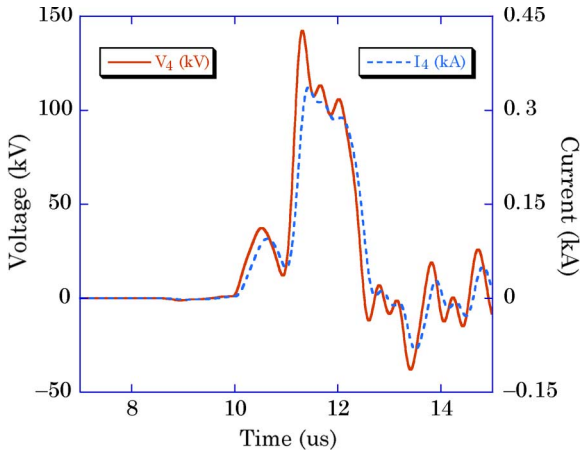


Fig. 12. Simulated waveforms of $V_4$ and $I_4$.

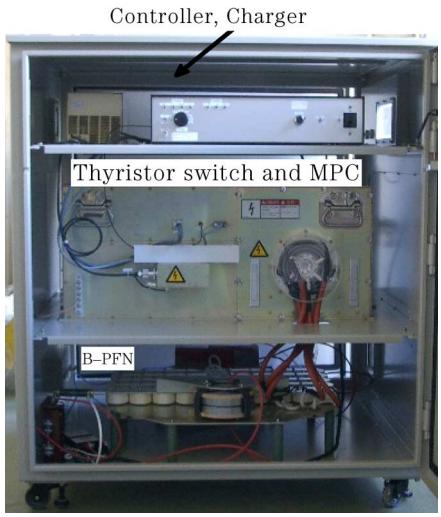


Fig. 13. Developed pulsed-power system in a cube box.

Fig. 12 shows the simulated output voltage and the current of the over all system. It can be seen that Peak 1 in Fig. 6 cannot be observed since the reset circuit for PT2 was modeled as a bypass with a switch in such a way of Fig. 7. By the proposed reset circuit, the undesirable Peak 1 was removed, whereas the charging of the BPFN was still valid. It is thought that the difference of the waveforms between the measured $I_4$ and the simulated $I_4$ is attributed to the fact that the experimental load consists of the matching resistor and the water discharge gap in parallel whereas the simulation load consists of only the matching resistor. The discharge gap in water can be dealt with by using the varying resistor and the varying capacitor in parallel as described in the earlier paper [10]. This fact encourages us to establish an EMTP model for the discharge gap in water.

## V. Streamerlike Discharge in Water

The developed pulsed-power system in all solid state is shown in Fig. 13. The volume and the weight of the system are about 1 m$^3$ and 150 kg, respectively. A relatively large volume ($\sim$34 cm$^3$) of streamer discharge was successfully generated in water with the developed system as shown in

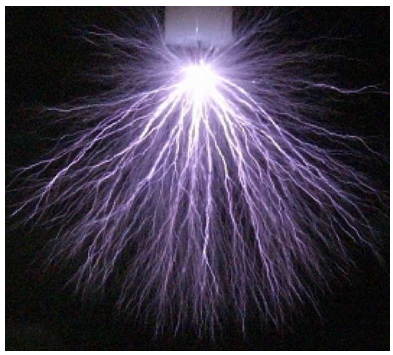

Fig. 14. Streamerlike discharge generated by the developed system in water. Electrode geometry: Needle to plane. Radius of curvature at the needle tip: 30 $\mu$m. Electrode gap: 100 mm. Tap-water conductivity: 25 mS/m.

Fig. 14. The streamer discharge is growing radially from the tip of the positive point electrode. The propagation distance of the streamer was measured as about 35 mm with the naked eyes. The streamerlike discharges generated by the developed system are supposed to be used for water treatments such as the sterilization of microorganisms and the decomposition of harmful materials.

## VI. Conclusion

A pulsed-power generator that can be operated with high repetition rate, long lifetime, and high reliability for industrial applications has been developed. The output voltage showed a peak voltage, rise time, and pulsewidth (FWHM) of about 140 kV, 200 ns, and 1 $\mu$s, respectively. The feasibility of EMTP simulation for more efficient design of the pulsed-power generator with MPC and BPFN was successfully studied with reasonable agreement with the experimental results. Water discharges were successfully generated with the developed system for practical industrial applications.

## References


[1] W. S. Melville, "The use of saturable inductors as discharge devices for pulse generators," *Proc. IEE*, vol. 98, pp. 185–207, 1951.

[2] W. C. Nunnally, "Magnetic switches and circuits," Los Alamos National Lab., Los Alamos, NM, LA-8862-MS, 1982.

[3] S. Nakajima, S. Arakawa, Y. Yamashita, and M. Shiho, "Fe-based nanocrystalline FINEMET cores for induction accelerators," *Nucl. Instrum. Methods Phys. Res. A, Accel. Spectrom. Detect. Assoc. Equip.*, vol. 331, no. 1–3, pp. 318–322, Jul. 1993.

[4] T. Sakugawa and H. Akiyama, "An all-solid-state pulsed power generator using a high-speed gate-turn-OFF thyristor and a saturable transformer," *Electr. Eng. Jpn.*, vol. 140, no. 4, pp. 17–26, 2002.

[5] W. Partlo, R. Sandstrom, and I. Fomenkov, "A low cost of ownership KrF excimer laser using a novel pulse power and chamber configuration," in *Proc. SPIE—Int. Soc. Opt. Eng.*, 1995, vol. 2440, p. 90.

[6] T. Namihira, S. Tsukamoto, D. Wang, S. Katsuki, R. Hackam, H. Akiyama, Y. Uchida, and M. Koike, "Improvement of NOx removal efficiency using short width pulsed power," *IEEE Trans. Plasma Sci.*, vol. 28, no. 2, pp. 434–442, Apr. 2000.

[7] Z. He, J. Liu, and W. Cai, "The important role of the hydroxy ion in phenol removal using pulsed corona discharge," *J. Electrost.*, vol. 63, no. 4, pp. 371–386, May 2005.

[8] E. Njatawidjaja, A. T. Sugiarto, T. Ohshima, and M. Sato, "Decoloration of electrostatically atomized organic dye by the pulsed streamer corona discharge," *J. Electrost.*, vol. 63, no. 4, pp. 353–359, May 2005.

[9] P. W. Smith, *Transient Electronics Pulsed Circuit Technology*. Hoboken, NJ: Wiley, 2002.

[10] Y. W. Choi *et al.*, "Analysis of the pulsed plasma reactor impedance for DeSOx and DeNOx," *Jpn. J. Appl. Phys.*, vol. 40, no. 2B, pp. 1108–1113, Feb. 2001.

[11] *Electromagnetic Transient Program (EMTP) Primer*, Palo Alto, CA: EPRI. EL-4202 Research Project 2149-1, Final Rep., 1985.

[12] *ATP Rule Book*, 2002, Buenos Aires, Argentina: Argentinian EMTP/ATP User group.


**Jaegu Choi** (M'05) was born in Kyoungpook, Korea, on March 16, 1969. He received the B.E. and M.E. degrees in electrical engineering from Kyoungpook National University, Daegu, Korea, in 1994 and 1996, respectively, and is currently working toward the Ph.D. degree at Kumamoto University, Kumamoto, Japan.

From 1996 to 2005, he was a Senior Researcher at the Korea Electrotechnology Research Institute, Changwon, Korea.

**Takahiro Yamaguchi** was born in Ehime, Japan, on May 23, 1981. He received the B.S. degree from Kumamoto University, Kumamoto, Japan, in 2004, where he is currently working toward the M.S. degree.

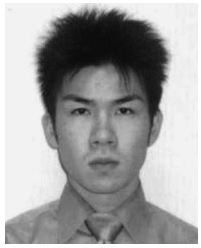

**Kunihiro Yamamoto** was born in Kumamoto, Japan, on September 26, 1982. He received the B.S. degree from Kumamoto University, Kumamoto, in 2005, where he is currently working toward the M.S. degree.

**Takao Namihira** (M'00–SM'05) was born in Shizuoka, Japan, on January 23, 1975. He received the B.S., M.S., and Ph.D. degrees from Kumamoto University, Kumamoto, Japan, in 1997, 1999, and 2003, respectively.

Since 1999, he has been a Research Associate with the Kumamoto University. During 2003–2004, he was on sabbatical leave at the Center for Pulsed Power and Power Electronics, Texas Tech University, Lubbock.

**Takashi Sakugawa** (M'00) received the M.E. degree from Kyushu University, Fukuoka, Japan, in 1989, and the D.E. degree from Kumamoto University, Kumamoto, Japan, in 2004.

He was with Meidensha Corporation from 1989 to 2004. He is currently an Associate Professor with Kumamoto University.

Prof. Sakugawa is a member of the Laser Society of Japan, the Institute of Electrostatics Japan, and the Japan Society of Applied Physics.

**Sunao Katsuki** (M'99) was born in Kumamoto, Japan, on January 5, 1966. He received the B.S., M.S., and Ph.D. degrees from Kumamoto University, Kumamoto, Japan, in 1989, 1991, and 1998, respectively.

From 1991 to 1998, he was a Research Associate with the Kumamoto University, where he is currently an Associate Professor. During 2001–2002, he was a Senior Researcher with the Plasma and Electronics Research Institute (PERI), Old Dominion University, Norfolk, VA.

**Hidenori Akiyama** (M'87–SM'99–F'00) received the Ph.D. degree from Nagoya University, Nagoya, Japan, in 1979.

From 1979 to 1985, he was a Research Associate with the Nagoya University. In 1985, he joined the faculty at Kumamoto University, Kumamoto, Japan, where he is currently a Professor.

Dr. Akiyama received the IEEE Major Education Innovation Award in 2000 and the IEEE Peter Haas Award in 2003.